Nanoscale

ROYAL SOCIETY OF CHEMISTRY

PAPER

View Article Online
View Journal | View Issue

Cite this: *Nanoscale*, 2015, **7**, 14469

Published on 28 July 2015. Downloaded by Universita Studi di Milano on 14/01/2016 14:25:15.

# Thermodynamic stability of high phosphorus concentration in silicon nanostructures

Michele Perego,*[a] Gabriele Seguini,[a] Elisa Arduca,[a,e] Jacopo Frascaroli,[a,e] Davide De Salvador,*[b,d] Massimo Mastromatteo,[b,d] Alberto Carnera,[b,d] Giuseppe Nicotra,[c] Mario Scuderi,[c] Corrado Spinella,[c] Giuliana Impellizzeri,[d] Cristina Lenardi[e] and Enrico Napolitani*[b,d]

Doping of Si nanocrystals (NCs) has been the subject of a strong experimental and theoretical debate for more than a decade. A major difficulty in the understanding of dopant incorporation at the nanoscale is related to the fact that theoretical calculations usually refer to thermodynamic equilibrium conditions, whereas, from the experimental point of view, impurity incorporation is commonly performed during NC formation. This latter circumstance makes impossible to experimentally decouple equilibrium properties from kinetic effects. In this report, we approach the problem by introducing the dopants into the Si NCs, from a spatially separated dopant source. We induce a P diffusion flux to interact with the already-formed and stable Si NCs embedded in $SiO_2$, maintaining the system very close to the thermodynamic equilibrium. Combining advanced material synthesis, multi-technique experimental quantification and simulations of diffusion profiles with a rate-equation model, we demonstrate that a high P concentration (above the P solid solubility in bulk Si) within Si NCs embedded in a $SiO_2$ matrix corresponds to an equilibrium property of the system. Trapping within the Si NCs embedded in a $SiO_2$ matrix is essentially diffusion limited with no additional energy barrier, whereas de-trapping is prevented by a binding energy of 0.9 eV, in excellent agreement with recent theoretical findings that highlighted the impact of different surface terminations (H- or O-terminated NCs) on the stability of the incorporated P atoms.

Received 21st April 2015,
Accepted 23rd July 2015

DOI: 10.1039/c5nr02584b

www.rsc.org/nanoscale

## Introduction

Semiconducting nanostructures with reduced dimensionality attract considerable scientific interest due to their peculiar properties arising from the interplay between quantum confinement and surface related effects. Si nanostructures are extremely appealing for applications in several fields like microelectronics, optoelectronics, photovoltaics, plasmonics and thermoelectrics.[1–4]

Their exploitation requires controlling the properties of these low dimensional materials by properly tuning the dopant concentration like in bulk semiconductors.[1,5–7] However, a clear understanding of dopant incorporation and subsequent activation at the nanoscale has not yet been achieved. In particular, the mechanisms involved in the dopant incorporation and solubility are different from those of bulk materials due to the increasing role of interfaces and of the surrounding matrix as the nanostructure size decreases.[8,9] Theoretical studies addressed the problem in a highly controversial manner, predicting different equilibrium configurations of the nanostructures.[10–13] Experimentally, high concentrations of dopants were introduced in low dimensional materials during their synthesis,[14,15] but a proper description of the physics of atomic transport at the nanoscale, and thus the validation of the existing theoretical models, has been prevented so far by the limitations of the experimental approaches. Key questions are: is dopant incorporation at the nanoscale allowed by thermodynamic stability, or is it a metastable condition that can be achieved only by the kinetic or non-equilibrium effect?[5,13] Can we measure the energy barriers describing atomic transport, *i.e.* the atomistic parameters provided also by calculations, thus linking experiments and theory?

Doping of Si nanocrystals (NCs) embedded in a $SiO_2$ matrix represents a paradigmatic system.[9,16,17] The attainable results

[a]Laboratorio MDM, IMM-CNR, Via Olivetti 2, I-20864 Agrate Brianza, Italy. E-mail: michele.perego@cnr.it
[b]Dipartimento di Fisica e Astronomia, Università degli Studi di Padova, Via Marzolo 8, I-35131 Padova, Italy. E-mail: davide.desalvador@unipd.it, enrico.napolitani@unipd.it
[c]IMM-CNR, Z. I. VIII Strada 5, I-95121 Catania, Italy
[d]MATIS IMM-CNR, Via S. Sofia 64, I-95132 Catania, Italy
[e]Dipartimento di Fisica, Università degli Studi di Milano, Via Celoria 23, I-20100 Milano, Italy

This journal is © The Royal Society of Chemistry 2015

Published on 28 July 2015. Downloaded by Universita Studi di Milano on 14/01/2016 14:25:15.

are in the extreme case of nanoscaling, *i.e.* from bulk to 0D systems, and therefore they are useful for the understanding of other systems with reduced dimensionality like nanowires, fins or nanosheets.[18–21] Furthermore, Si NCs were the subject of an intense research activity due to their optical and electronic properties.[22] This effort was supported by the concomitant development of a technology to place Si NCs within the $SiO_2$ matrix with nanometer accuracy, resulting in the formation of an array of NCs with a well-controlled average diameter and narrow size distribution.[23,24]

Doping of Si NCs in a $SiO_2$ matrix was performed by introducing the dopant in the matrix before NC formation and subsequently inducing dopant incorporation and Si NC formation simultaneously.[14,25–30] This approach indicated that inclusion of electrically active impurities in Si NCs is kinetically possible (*e.g.* due to the lack of diffusion), and highlighted the corresponding modification of the NC band structure.[15,26,29,31] However, these results do not provide any information on the energetics of atomic transport at the NCs since the experiments were conducted out of equilibrium. Moreover, the presence of impurities during the Si NC synthesis significantly affects the growth kinetics leading to size variations of the resulting nanoparticles.[31] This effect partially accounts for discrepancies in the experimental evidence reported in the literature.[31–36] From a theoretical point of view, we must distinguish between the studies that investigate H-terminated Si NCs and those that consider the effect of the surrounding $SiO_2$ matrix. Seminal work by Chelikowsky's group showed evidence of B and P segregation at the surface of H-terminated Si NCs and proposed the occurrence of a self-purification mechanism in NCs with $d$ < 2 nm.[13,37–39] Recently several authors have unambiguously demonstrated that this result cannot be transferred to O-terminated Si NCs: if the $SiO_2$ matrix is taken into account, incorporated P has a minimum of binding energy in the inner part or in the sub-interface region of the Si nanoclusters, suggesting the possibility to stably incorporate impurities within the Si NCs. However, a consensus on the effective binding energy values is still lacking with theoretical prediction ranging from 1 to 4 eV.[11,12,21,40]

In this work, we describe the atomic transport properties governing the P incorporation within Si NCs embedded in a $SiO_2$ matrix. The incorporation of P atoms is promoted in Si NCs after their formation, by delivering a controlled amount of dopant atoms from a spatially separated diffusion source. In this way, the energetics of trapping/detrapping of P in the NCs are measured at equilibrium and modelled as a function of the annealing temperature and time, avoiding kinetic effects due to NC formation. This experimental approach allows comparing the experimental results with existing theoretical data. In agreement with recent calculations on O-terminated NCs, P is shown to be incorporated within the NCs, at concentrations well above the P solubility in bulk Si. Besides the fundamental issues on doping processes, the experiment and modelling results suggest that the historical doping method by diffusion could be reconsidered at the nanoscale for high doping of future nanostructured devices.

# Experimental

Si NCs were synthesized by e-beam evaporation on a p-type Si substrate of a SiO film (6.2 nm) between two $SiO_2$ layers. Furnace annealing (1150 °C, 1 hour, $N_2$) promoted phase separation and Si NC formation. Subsequently, a thin (0.4 nm) layer of P–$SiO_2$ was evaporated,[14] on top of the tri-layered structure and *in situ* capped with a 20 nm thick $SiO_2$ film. A reference sample was also prepared by depositing the P–$SiO_2$ layer and the 20 nm thick $SiO_2$ capping layer on top of a $SiO_2$ layer without Si NCs. High temperature thermal treatment to promote P diffusion and trapping was performed in a tubular furnace at a temperature ($T_{ANN}$) ranging from 900 °C to 1100 °C under a $N_2$ atmosphere. The annealing time ($t_{ANN}$) was varied between 30 min and 16 hours.

Energy filtered transmission electron microscopy (EFTEM) cross sectional and plan view images of the sample were obtained on a JEOL JEM 2010F system operated at 200 keV. Time of Flight Secondary Ion Mass Spectrometry (ToF-SIMS) analysis was performed using a dual beam ION-ToF IV system. Sputtering was accomplished by $Cs^+$ ions at 1 keV and 80 nA. The analysis was performed in negative polarity by using $Ga^+$ ions operating at 25 keV and 1 pA. During the analysis, the samples were charge compensated by means of an electron flood gun. Accurate time-to-depth conversion was performed by measuring the average sputter velocity in the oxide. A calibration of the $^{31}P^-$ signals was obtained measuring the total P dose in samples by Rutherford Backscattering Spectrometry (RBS) and nuclear reaction analysis (NRA) and applying the protocols reported elsewhere.[41] RBS analyses were performed at Laboratori Nazionali di Legnaro (LNL, Italy) by using 3 MeV $^4He^+$ beams delivered by the CN Van de Graaff accelerator. The Rutherford $^{31}P(\alpha,el)^{31}P$ reaction was used with a scattering angle of 165°–170° with the substrate under [100] channelling conditions. A cross check was performed by means of a nuclear reaction analysis $^{31}P(\alpha,p_0)^{34}S$ at 5 MeV using the InP bulk sample as a reference for cross section calibration. P doses were obtained with relative errors in the 6–8% range for the most significative samples. X-ray Photoelectron Spectroscopy (XPS) measurements were performed on a PHI 5600 system using a monochromatic Al $K_\alpha$ = 1486.6 eV X-ray source and a concentric hemispherical analyser with a nominal energy resolution of 0.5 eV. The spectra were collected at a take-off angle of 80°. The C 1s line at 285 eV was used as a reference to correct the charge shift of the binding energies.

# Results

Fig. 1 shows the EFTEM cross sectional (Fig. 1a, background) and plan view images (Fig. 1b). The cross sectional image indicates that the Si NCs are aligned in a 2D layer with a thickness of (3.9 ± 0.6) nm and a well-controlled distance from the Si substrate. From the plan view images, we measured an average diameter ($d$) of (4.0 ± 0.6) nm and an average areal density ($N$) of $1.3 \times 10^{12}$ dots per $cm^2$. Fig. 1c (green histogram) shows the

 This journal is © The Royal Society of Chemistry 2015

Published on 28 July 2015. Downloaded by Universita Studi di Milano on 14/01/2016 14:25:15.

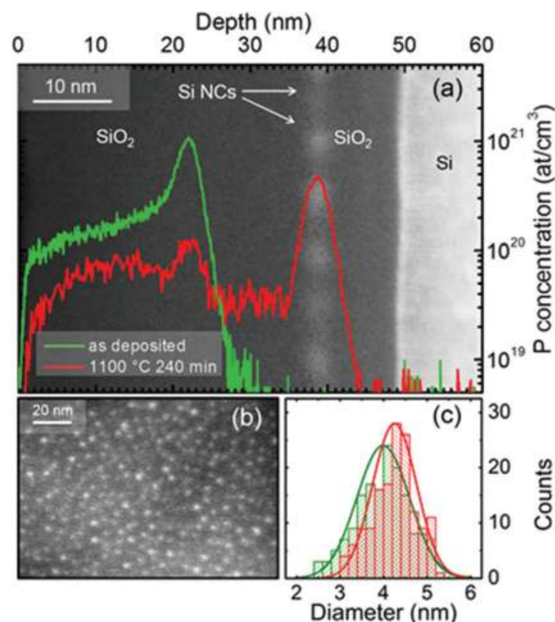


**Fig. 1** (a) ToF-SIMS profiles of the as deposited (green) and annealed (1100 °C, 4 hours, red) samples overlapped with the EFTEM cross sectional image of the as deposited sample. (b) EFTEM plan view image of the as deposited sample. (c) NC size distribution of the as deposited (green) and annealed (red) sample as obtained from the EFTEM plan view images.

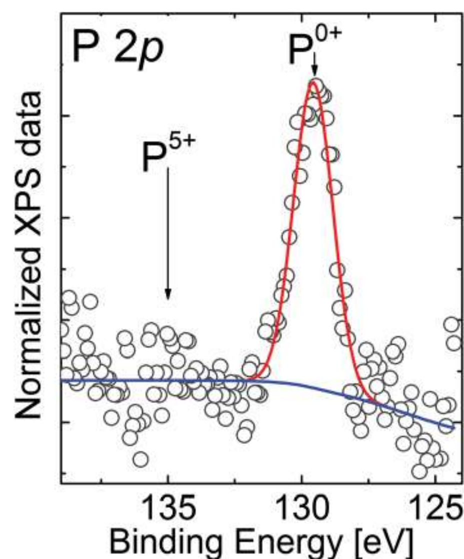


**Fig. 2** High-resolution XPS spectrum of the P 2p core level signal after subtraction of the Si 2p plasmon loss signal for the annealed sample (1100 °C, 4 hours).

corresponding size distribution. Fig. 1a shows the calibrated ToF-SIMS $^{31}P^-$ signals.[41–44] The $^{31}P^-$ profiles are overlapped with the cross sectional EFTEM image. The starting profile (green line) has a shallow peak at a depth of 22 nm well separated by the NC zone, with a trailing edge due to residual P atoms in the deposition chamber.

The samples were further annealed under a $N_2$ atmosphere at 900, 1000 or 1100 °C for $t_{ANN}$ ranging from 30 min to 16 hours. The EFTEM plan view analysis of the annealed sample (1100 °C, 4 hours) indicates that $d = (4.2 \pm 0.5)$ nm and $N = 1.5 \times 10^{12}$ dots per cm$^2$. Fig. 1c (red histogram) shows the corresponding Si NC size distribution. These data demonstrate that the Si NCs were not affected by subsequent annealing at lower temperature. Fig. 1a (red line) shows the corresponding $^{31}P^-$ profile, exhibiting significant diffusion in the oxide and segregation in the NC region. No P accumulation in the $SiO_2$ layer between the Si NCs and the Si substrate is observed, suggesting that the Si NC layer efficiently traps the diffusing P atoms.

Fig. 2 shows the XPS high-resolution spectrum of the P 2p core level signal for the annealed sample (1100 °C, 4 hours). The $SiO_2$ capping layer was thinned down (2 nm) by calibrated HF etching before XPS analysis. The final structure of the sample after the etching process was monitored by ToF-SIMS depth profiling. The P 2p spectral line was fitted by a simple Voigt function. The loss structure of the intense Si 2p signal located at 100 eV was modelled with a broad Gaussian profile and subtracted to highlight the P 2p signal. The position of the P 2p spectral line is determined to be (129.6 ± 0.03) eV and the FWHM of the fitting function is 1.7 eV. P atoms in the $SiO_2$ matrix correspond to a P 2p signal at ≈135 eV, while P atoms in a Si matrix exhibit a P 2p signal at ≈129 eV.[14,45] The XPS data demonstrate that, during the annealing process, the diffusing P atoms are trapped in the Si NC region and incorporated in the core of the nanostructure or in a sub-interface region exhibiting no bonds with O atoms. The sensitivity of the XPS measurements does not allow excluding the presence of a residual amount of P in the surrounding $SiO_2$ matrix. Nevertheless on the basis of the calibrated ToF-SIMS profiles we can estimate that the concentration of P atoms in the $SiO_2$ film is of the order of $10^{19}$ atoms per cm$^3$, corresponding to a very limited fraction of the total amount of phosphorus trapped in the NC region.

Fig. 3 shows the calibrated ToF-SIMS profiles of the samples after isothermal treatments performed at 900 °C (a), 1000 °C (b) and 1100 °C (c). They provide a clear insight into the dynamics of the trapping process. On increasing the thermal budget, more P atoms diffuse through the $SiO_2$ matrix and segregate in the Si NC region. Since the capturing flux depends on the diffusivity in $SiO_2$, that is a thermal activated process, the maximum concentration in the NC layer at 1000 °C is less than that at 1100 °C, and it further decreases by two orders of magnitude at 900 °C. It is also worth noting that a P diffusion gradient from the NCs towards the surface becomes visible after 16 hours at 1100 °C. This clearly indicates that not only capture comes into play, but also the release of P atoms from NCs.

The P areal density in the NCs ($\Phi$) is computed by integrating the peak of the $^{31}P^-$ profiles at the NCs. The ratio $\Phi/N$ gives the average number of P atoms trapped within a single NC structure, while dividing by the average number of

Published on 28 July 2015. Downloaded by Universita Studi di Milano on 14/01/2016 14:25:15.

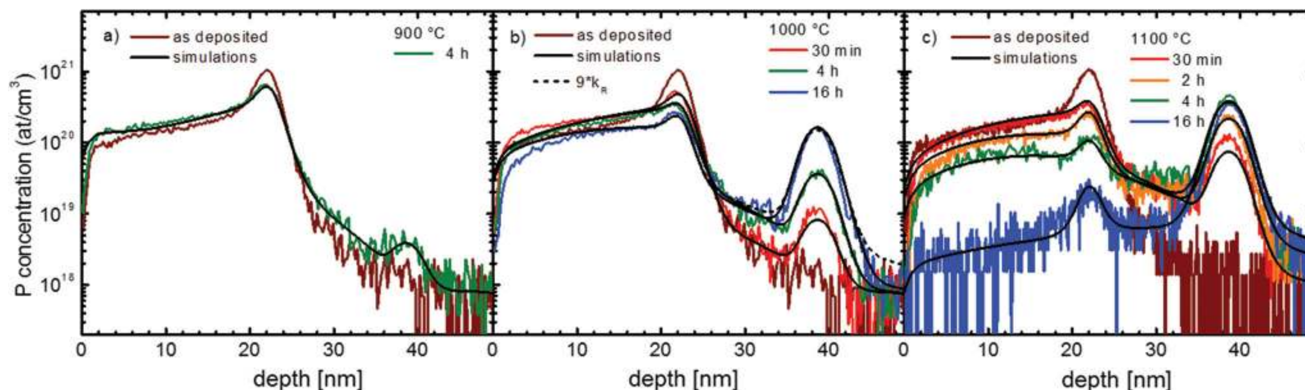


**Fig. 3** P concentration profiles for different annealing times (coloured lines) and corresponding simulation fittings (black lines) at 900 °C (a), 1000 °C (b) and 1100 °C (c). Simulation considering $k_R$ at ×9 of the best-fit value is shown (black dashed line) in (b).

Si atoms per NC we get the atomic fraction (percentage) of P within Si NCs:

$$C_P^{NCs}(at\%) = \frac{\Phi}{N}\frac{100}{C_{Si}V} \tag{1}$$

where $C_{Si}$ is the Si atomic density and $V$ is the average volume of the clusters in the approximation of the spherical shape. Fig. 4 shows $\Phi/N$ (left axis) and $C_P^{NCs}$ (right axis) values as deduced by ToF-SIMS and TEM data as a function of $t_{ANN}$ in the case of the isothermal treatments at 1100 °C and 1000 °C. A progressive increase of P concentration in the Si NCs is observed when raising the $t_{ANN}$ up to 4 hours at 1100 °C, where the trapping mechanism allows achieving a very high P concentration within the Si NCs of about 6%. This value largely exceeds the solid solubility for P in bulk Si.[46] For longer annealing (16 hours), the diffusion source strongly diminishes while the amount of P in NCs reduces only slightly, demonstrating the strong stability of the P atoms incorporated into the Si NCs. At 1000 °C, P diffusion across $SiO_2$ is lower and, as a consequence, only the P concentration increase is observed. The P concentration within the Si NCs is about 2%, which is lower than in the sample annealed at 1100 °C, but higher than the bulk Si solubility.

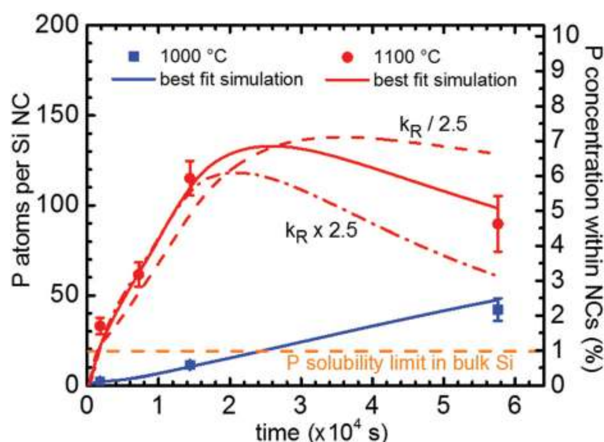


**Fig. 4** Experimental P concentration inside the NCs as a function of time at 1000 °C (blue squares) and at 1100 °C (red circles). Continuous lines come from the numerical simulations based on the rate equation model. Simulations obtained fixing $k_R$ at /2.5 (dashed curve) and ×2.5 (dashed-dotted curve) of the best-fit value are also shown.

These experimental results provide an evident picture of the doping incorporation in Si NCs very close to equilibrium in the diffusion process. Quantitative physical information about the energetics of the system can be extracted by fitting the ToF-SIMS profiles using a diffusion model based on Fick's law in one dimension.[46] The three fluxes describing the P interaction with NCs are

– capturing flux: $-k_C DNA(c^+ + c^-)$, describing the capturing process at NCs,

– release flux: $k_R\Phi$, describing the release of P in the $SiO_2$ matrix from the NCs,

– diffusion flux through the uncovered area: $(1 - NA)D\partial c/\partial x$, considering that P diffuses only through the fraction of the layer uncovered by NCs,

where $c^+$ and $c^-$ are the P concentrations just before and after the NC layer along the growth direction $x$, $A$ is the average cluster area and $NA$ is the coverage fraction of the NCs in the layer, and $D$ is the P diffusivity in the $SiO_2$. $k_C$ and $k_R$ quantify respectively the capturing efficiency of the clusters and the rate at which a single P atom escapes from the clusters. Continuity equations are applied to the P fluxes to obtain the concentration in $SiO_2$ as a function of depth and time as well as the $\Phi$ value as a function of time. $D$ in the oxide containing the clusters, and the constants $k_C$ and $k_R$ are the only free fundamental atomistic parameters of the model, the coverage fraction $NA \approx 0.2$ being determined by the experimental EFTEM and the boundary conditions being determined by using ToF-SIMS data in a $SiO_2$ reference without NCs. A single set of these three parameters is optimized for all the different times at a specific temperature by minimizing a cumulative chi-square function. The same procedure allowed also estimation of the errors of the parameters.


This journal is © The Royal Society of Chemistry 2015

Published on 28 July 2015. Downloaded by Universita Studi di Milano on 14/01/2016 14:25:15.

Fig. 3 shows good fitting of experimental ToF-SIMS P profiles at each $T_{ANN}$ (black continuous lines). The agreement between the total amount of P in NCs and the simulation (Fig. 4) is even better, because the integrated amount of P is not affected by slight fluctuation in the ToF-SIMS resolution. Data points show the error bars deduced by ToF-SIMS repeatability and calibration. At 1100 °C, the capture prevails during the first 7 hours and then release becomes visible due to the source exhaustion. The release process causes the change in the slope and this is correctly reproduced by the simulations. At 1000 °C the thermal budget is lower and capture prevails at all the investigated temperatures.

The capturing constant is determined to be $k_C \approx 25\ nm^{-1}$, irrespective of the $T_{ANN}$. This is a high value that forces the simulations to make the trapping process prevailing over release for short annealing times during which no P crosses the NC region through the uncovered fraction of the NC layer. Smaller trapping would allow populating with P the region between the clusters and the substrate also during the first annealing times. The single $k_C$ value used to fit data of all temperatures demonstrates that no significant capture barrier (additional to the diffusion barrier) is present and that trapping is diffusion limited.

Diffusivity values obtained by the fitting of the experimental data are more easily discussed calculating the diffusivity rate $k_D$, *i.e.* the jumping frequency of P atoms as defined by:

$$D = \frac{a^2}{6} \times k_D \quad (2)$$

where $a$ is the length of each diffusion step ($a \approx 0.35$ nm the average distance between $SiO_2$ molecules). Fig. 5 shows $k_D$ values at different temperatures for the samples with NCs and for the $SiO_2$ reference. The same plot shows $k_R$ values as deduced by the $^{31}P^-$ profile fitting.

Direct evidence of the sensitivity of the release rate at 1100 °C is reported in Fig. 4, where we show also two simulations obtained by repeating the whole fitting procedure of the ToF-SIMS profiles by fixing $k_R$ at /2.5 (dashed curve) and ×2.5 (dashed-dotted curve) of the best fit value (*i.e.* corresponding to the minimum and maximum values, respectively, after doubling the error bars on the log scale in Fig. 5). It is clear that these latter curves do not correctly describe the experimental data. At 1000 °C the thermal budget is too low to have a P release significantly affecting the P concentration in the NCs and consequently the sensitivity of $k_R$ on the simulations is much lower. However, the release of P from NCs causes also the change of the P concentration in $SiO_2$ beyond the NCs (*i.e.* depths between 45 and 50 nm in Fig. 3b). In order to evidence the sensitivity of $k_R$ on the simulations at 1000 °C we have included in Fig. 3b a simulation (dashed curve) obtained by assuming $k_R$ at ×9 of the best fit value. This corresponds to the maximum value after doubling the upper error bar on the log scale in Fig. 5. The resulting simulated profile does not correctly describe the data. At lower values assuming $k_R = 0$ the simulation (not shown) still satisfactorily fit the data within errors considering the counting Poisson statistics of ToF-SIMS yield. No useful data can be instead deduced for $k_R$ at 900 °C.

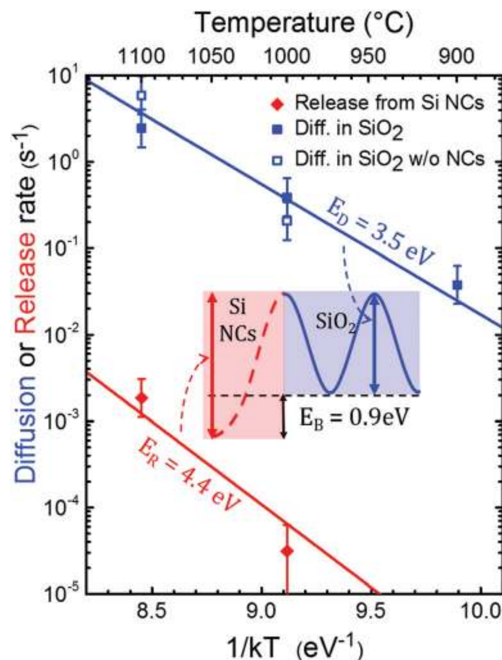


Fig. 5 Diffusion (release) rates are reported with filled blue squares (red). The lower error bar of the release rate at 1000 °C corresponds to 100% of the best-fit value. Data relative to reference $SiO_2$ samples are reported (blue). The Arrhenius fit of experimental diffusion (release) rates is reported (solid line). The inset depicts the entire energy scheme.

As can be noted in Fig. 5, a P atom leaves the cluster with a much smaller frequency than the one regulating its diffusion jump: more than 4 orders of magnitude slower. Diffusivity (release) rates are well fitted by Arrhenius' formula:

$$k_{D(R)} = k_0 \exp(-E_{D(R)}/kT) \quad (3)$$

using a single $k_0 = 1.9 \times 10^{13}\ s^{-1}$ that is the attempt frequency with no barrier (in the high temperature limit), a diffusion barrier $E_D = 3.5$ eV, and a higher release barrier $E_R = 4.4$ eV.

The inset of Fig. 5 summarizes the energy scheme for the P–NC interaction. P is thermodynamically favoured to be trapped at NCs with a binding energy of

$$E_B = E_R - E_D = (0.9 \pm 0.1)\ eV \quad (4)$$

## Discussion

Since Si NCs do not evolve during P diffusion and the P trapping process occurs without perturbing the original nanostructures, our experimental and modelling analysis depicts an interesting scenario of the system close to equilibrium. In our system P atoms are incorporated within the Si NCs, and not at their surface as demonstrated by XPS analysis. The experimental data strongly support the theoretical papers that underline the role of the surrounding matrix in describing the P

Published on 28 July 2015. Downloaded by Universita Studi di Milano on 14/01/2016 14:25:15.

stability into the clusters.[11,12,21,40] At variance with respect to the experimental and theoretical papers working on a H-terminated system[47,48] we find that P incorporation is energetically favoured in NCs when O-termination is adopted.

From a quantitative point of view, our experimental layout supports also a straightforward correlation with the theoretical calculations that consider the role of the embedding matrix. Carvalho *et al.*[11] determined a binding energy of 3 eV using silanol groups to simulate the oxide at the surface of the Si NCs. Similarly, Guerra *et al.*[21] found a value of 4 eV considering a more extended $SiO_2$ shell. Both data largely exceed our experimental value. Using a more complex model, Ni *et al.*[40] recently pointed out the role of dangling bonds at the $Si/SiO_2$ interface, suggesting that they may facilitate the incorporation of P in Si NCs embedded in $SiO_2$ with a binding energy of 1 eV, in perfect agreement with our finding.

Moreover, the maximum measured P concentration in NCs, which was 6% at 1100 °C, is significantly higher than the P solubility limit in bulk Si (0.4–1.0% in the 900–1100 °C range).[46] At 900 °C and 1000 °C, we observed lower maximum concentrations but this is ascribed to the reduced flux of P towards the NCs rather than a reduced solubility. Nanoscale solubility appears thus to be more than 6 times higher than the bulk one. This is a lower level estimate of P solubility in Si NCs: using the model parameters to calculate the equilibrium steady state between capture and release with a non-exhaustive source, the P concentration in NCs might increase up to 20%. This result suggests that solubility of dopants increase by reducing the semiconductor size, at least down to the investigated size ($d \approx 4$ nm). This is in striking contrast to theoretical models predicting self-purification phenomena,[5,37–39,49] and experiments far from equilibrium.[15,31,32,47,48] It is worth considering that all the calculations predicting the P solubility in Si NCs consider H-termination of the nanostructures, and they consequently suggest a decrease of the solubility with decreasing cluster size. In our experiment Si NCs are O-terminated accounting for the discrepancy with the calculations and indicating that, also in this case, a significant role of surface termination is played in the equilibrium solubility of dopants at the nanoscale. From an experimental point of view, Gnaser *et al.*[32] showed a decrease, with cluster size, of the P concentration in NCs during their formation. According to our model, the reported trend indicates that, very likely, small clusters kinetically trap less P than bigger ones due to their small capture area, but this does not demonstrate that at equilibrium smaller clusters can absorb less P atoms.

It is worth remembering that impurity incorporation within the semiconductor does not automatically imply effective doping of the semiconductor since activation of the dopants is required. The latter issue has been addressed in a recent publication providing an indication about the predominant incorporation of P atoms in interstitial sites within the Si NCs.[50] According to standard (bulk) knowledge of semiconductor doping this would imply that P hardly ionizes and cannot be active to introduce electrons into the conduction band of the nanostructure. On the other hand, direct measurements of dopant activation in very small semiconductor nanostructures have not been reported in the literature so far and therefore a complete picture of nanoscale doping has not been provided yet. Nevertheless the capability to tune the P content in the Si NCs over a broad range of concentrations – as demonstrated in this paper – is a fundamental prerequisite to test the effective activation of the incorporated dopants.

## Conclusions

In conclusion, by decoupling Si NC synthesis from P diffusion/trapping, we demonstrated that P doping of Si NCs in $SiO_2$ corresponds to a thermodynamically favoured configuration of the system. The P concentration is at least 6 times the solubility in the bulk material, suggesting an increase of solubility in Si nanostructures. High levels of impurities can be introduced in the inner part of Si NCs in a stable configuration and the dopant content can be finely tuned by properly adjusting the annealing conditions. Furthermore, a mesoscopic modelling of the experimental data provides the first estimate of the P binding energy in Si NCs, to be compared with the existing *ab initio* calculations. This approach discloses opportunities for fundamental studies concerning the physics of low dimensional semiconductors and for their technological exploitation in nanostructured devices. As a matter of fact the experimental results suggest that the same diffusion processes that were largely used in the past for bulk systems could represent a viable solution towards high doping in nanostructures. This approach could be particularly appealing in conjunction with monolayer doping processes to control the amount of dopants introduced in nanostructured systems.

## Acknowledgements

Mario Alia (MDM, IMM-CNR) is acknowledged for technical assistance during evaporation and thermal processing. Luca Bacci and Luca Maran (University of Padova) are acknowledged for technical assistance during RBS/NRA measurements. Nicolò Sartori (University of Padova) is acknowledged for his support in part of the simulation activity.

## References

1 R. Gresback, N. J. Kramer, Y. Ding, T. Chen, U. R. Kortshagen and T. Nozaki, *ACS Nano*, 2014, **8**, 5650.
2 F. Priolo, T. Gregorkiewicz, M. Galli and T. F. Krauss, *Nat. Nanotechnol.*, 2014, **9**, 19.
3 J. Tang, H.-T. Wang, D. H. Lee, M. Fardy, Z. Huo, T. P. Russell and P. Yang, *Nano Lett.*, 2010, **10**, 4279.
4 M. C. Beard, K. P. Knutsen, P. Yu, J. M. Luther, Q. Song, W. K. Metzger, R. J. Ellingson and A. J. Nozik, *Nano Lett.*, 2007, **7**, 2506.
5 D. J. Norris, A. L. Efros and S. C. Erwin, *Science*, 2008, **319**, 1776.


This journal is © The Royal Society of Chemistry 2015

6 E. Prati, M. Hori, F. Guagliardo, G. Ferrari and T. Shinada, *Nat. Nanotechnol.*, 2012, **7**, 443.
7 Y. Shimizu, H. Takamizawa, K. Inoue, F. Yano, Y. Nagai, L. Lamagna, G. Mazzeo, M. Perego and E. Prati, *Nanoscale*, 2014, **6**, 706.
8 A. Puzder, A. Williamson, J. Grossman and G. Galli, *Phys. Rev. Lett.*, 2002, **88**, 097401.
9 G. Seguini, C. Castro, S. Schamm-Chardon, G. BenAssayag, P. Pellegrino and M. Perego, *Appl. Phys. Lett.*, 2013, **103**, 023103.
10 A. Carvalho, S. Öberg, M. J. Rayson and P. R. Briddon, *Phys. Rev. B: Condens. Matter*, 2012, **86**, 045308.
11 A. Carvalho, S. Öberg, M. Barroso, M. J. Rayson and P. Briddon, *Phys. Status Solidi A*, 2012, **209**, 1847.
12 A. Carvalho, M. J. Rayson and P. R. Briddon, *J. Phys. Chem. C*, 2012, **116**, 8243–8250.
13 T.-L. Chan, M. L. Tiago, E. Kaxiras and J. R. Chelikowsky, *Nano Lett.*, 2008, **8**, 596.
14 M. Perego, C. Bonafos and M. Fanciulli, *Nanotechnology*, 2010, **21**, 025602.
15 D. J. Rowe, J. S. Jeong, K. A. Mkhoyan and U. R. Kortshagen, *Nano Lett.*, 2013, **13**, 1317.
16 K. Seino, F. Bechstedt and P. Kroll, *Phys. Rev. B: Condens. Matter*, 2010, **82**, 085320.
17 G. Hadjisavvas and P. Kelires, *Phys. Rev. Lett.*, 2004, **93**, 226104.
18 K. E. Moselund, H. Ghoneim, H. Schmid, M. T. Björk, E. Lörtscher, S. Karg, G. Signorello, D. Webb, M. Tschudy, R. Beyeler and H. Riel, *Nanotechnology*, 2010, **21**, 435202.
19 G. Petretto, A. Debernardi and M. Fanciulli, *Nano Lett.*, 2013, **13**, 4963.
20 N. Fukata, J. Kaminaga, R. Takiguchi, R. Rurali, M. Dutta and K. Murakami, *J. Phys. Chem. C*, 2013, **117**, 20300.
21 R. Guerra and S. Ossicini, *J. Am. Chem. Soc.*, 2014, **136**, 4404.
22 L. Pavesi and R. Turan, *Silicon Nanocrystals, Fundamentals Synthesis and Application*, Wiley-VCH, Berlin, 2010.
23 C. Bonafos, M. Carrada, N. Cherkashin, H. Coffin, D. Chassaing, G. Ben Assayag, A. Claverie, T. Muller, K. H. Heinig, M. Perego, M. Fanciulli, P. Dimitrakis and P. Normand, *J. Appl. Phys.*, 2004, **95**, 5696.
24 M. Zacharias, J. Heitmann, R. Scholz, U. Kahler, M. Schmidt and J. Bläsing, *Appl. Phys. Lett.*, 2002, **80**, 661.
25 M. Perego, G. Seguini and M. Fanciulli, *Surf. Interface Anal.*, 2013, **45**, 386.
26 M. Fujii, A. Mimura, S. Hayashi, K. Yamamoto, C. Urakawa and H. Ohta, *J. Appl. Phys.*, 2000, **87**, 1855.
27 M. Fujii, A. Mimura, S. Hayashi, Y. Yamamoto and K. Murakami, *Phys. Rev. Lett.*, 2002, **89**, 206805.
28 M. Fujii, K. Toshikiyo, Y. Takase, Y. Yamaguchi and S. Hayashi, *J. Appl. Phys.*, 2003, **94**, 1990.
29 M. Fujii, Y. Yamaguchi, Y. Takase, K. Ninomiya and S. Hayashi, *Appl. Phys. Lett.*, 2004, **85**, 1158.
30 F. Ruffino, L. Romano, E. Carria, M. Miritello, M. G. Grimaldi, V. Privitera and F. Marabelli, *J. Nanotechnol.*, 2012, **2012**, 1.
31 R. Khelifi, D. Mathiot, R. Gupta, D. Muller, M. Roussel and S. Duguay, *Appl. Phys. Lett.*, 2013, **102**, 013116.
32 H. Gnaser, S. Gutsch, M. Wahl, R. Schiller, M. Kopnarski, D. Hiller and M. Zacharias, *J. Appl. Phys.*, 2014, **115**, 034304.
33 G. Kachurin, S. G. Cherkova, V. Volodin, V. G. Kesler, A. K. Gutakovsky, A. G. Cherkov, A. V. Bublikov and D. I. Tetelbaum, *Nucl. Instrum. Methods Phys. Res., Sect. B*, 2004, **222**, 497.
34 A. I. Belov, V. A. Belyakov, V. A. Burdov, A. N. Mikhailov and D. I. Tetelbaum, *J. Surf. Invest.: X-Ray, Synchrotron Neutron Tech.*, 2009, **3**, 527.
35 G. A. Kachurin, S. G. Cherkova, V. A. Volodin, D. M. Marin, D. I. Tetelbaum and H. Becker, *Semiconductors*, 2006, **40**, 72.
36 A. N. Mikhaylov, D. I. Tetelbaum, V. A. Burdov, O. N. Gorshkov, A. I. Belov, D. A. Kambarov, V. A. Belyakov, V. K. Vasiliev, A. I. Kovalev and D. M. Gaponova, *J. Nanosci. Nanotechnol.*, 2008, **8**, 780.
37 T. L. Chan, S. B. Zhang and J. R. Chelikowsky, *Appl. Phys. Lett.*, 2011, **98**, 133116.
38 G. Dalpian and J. Chelikowsky, *Phys. Rev. Lett.*, 2006, **96**, 226802; G. Dalpian and J. Chelikowsky, *Phys. Rev. Lett.*, 2008, **100**, 179703.
39 T.-L. Chan, A. Zayak, G. Dalpian and J. Chelikowsky, *Phys. Rev. Lett.*, 2009, **102**, 025901.
40 Z. Ni, X. Pi and D. Yang, *Phys. Rev. B: Condens. Matter*, 2014, **89**, 035312.
41 M. Mastromatteo, E. Arduca, E. Napolitani, G. Nicotra, D. De Salvador, L. Bacci, J. Frascaroli, G. Seguini, M. Scuderi, G. Impellizzeri, C. Spinella, M. Perego and A. Carnera, *Surf. Interface Anal.*, 2014, **46**, 393.
42 R. G. Wilson, F. A. Stevie and C. W. Magee, *Secondary Ion Mass Spectrometry: A Practical Handbook for Depth Profiling and Bulk Impurity Analysis*, Wiley, New York, 1989.
43 M. Perego, S. Ferrari, M. Fanciulli, G. Ben Assayag, C. Bonafos, M. Carrada and A. Claverie, *J. Appl. Phys.*, 2004, **95**, 257.
44 M. Perego, S. Ferrari, S. Spiga, E. Bonera, M. Fanciulli and V. Soncini, *Appl. Phys. Lett.*, 2003, **82**, 121.
45 A. I. Kovalev, D. L. Wainstein, D. I. Tetelbaum, W. Hornig and Y. N. Kucherehko, *Surf. Interface Anal.*, 2004, **36**, 959.
46 P. Pichler, *Intrinsic Point Defects, Impurities, and Their Diffusion in Silicon*, Computational Microelectronics, ed. S. Seiberherr, Springer, Wien, NewYork, 2004.
47 X. D. Pi, R. Gresback, R. W. Liptak, S. A. Campbell and U. Kortshagen, *Appl. Phys. Lett.*, 2008, **92**, 123102.
48 A. R. Stegner, R. N. Pereira, R. Lechner, K. Klein, H. Wiggers, M. Stutzmann and M. S. Brandt, *Phys. Rev. B: Condens. Matter*, 2009, **80**, 165326.
49 T.-L. Chan, H. Kwak, J.-H. Eom, S. B. Zhang and J. R. Chelikowsky, *Phys. Rev. B: Condens. Matter*, 2010, **82**, 115421.
50 D. König, S. Gutsch, H. Gnaser, M. Wahl, M. Kopnarski, J. Göttlicher, R. Steininger, M. Zacharias and D. Hiller, *Sci. Rep.*, 2015, **5**, 9702.

Published on 28 July 2015. Downloaded by Universita Studi di Milano on 14/01/2016 14:25:15.